Journal of Catalysis **202,** 45–58 (2001)
doi:10.1006/jcat.2001.3251, available online at http://www.idealibrary.com on IDEAL®

The Structure of Active Sites in *Me*–V–O Catalysts (*Me* = Mg, Zn, Pb) and Its Influence on the Catalytic Performance in the Oxidative Dehydrogenation (ODH) of Propane

P. Rybarczyk, H. Berndt, J. Radnik, M.-M. Pohl, O. Buyevskaya, M. Baerns, and A. Brückner[1]

Institut für Angewandte Chemie Berlin-Adlershof e. V., Richard-Willstätter-Straße 12, D-12489 Berlin, Germany

Received November 10, 2000; revised April 21, 2001; accepted April 21, 2001

***Me*–V–O catalysts (*Me* = Mg, Zn, Pb) of different Me : V ratios were characterized with respect to phase composition, structure and valence state of vanadium sites as well as composition and acid–base properties of the surface using XRD, TEM, TPR, TPD/TPRS, FTIR, potentiometric titration, XPS, EPR, and UV/VIS-DRS. The latter two techniques were also applied *in situ* under catalytic reaction conditions. The following structure–reactivity relationships were derived by comparing the results of catalyst characterization with those of catalytic tests: Both V^{5+} and V^{4+} catalyze the ODH of propane; however, V^{4+} seems to be more selective though less active than V^{5+}. V sites in octahedral or square pyramidal coordination are more active but less selective than VO_4 tetrahedra. Isolated VO_4 and V_2O_7 units as present in crystalline metal ortho- and pyrovanadates, respectively, are more selective but less active than VO_x species in amorphous clusters or even in crystalline chain- or layer-like structures. The differences in the catalytic properties arising from different metal cations are governed not only by the oxidation potential of the latter but also to a major degree by the acid–base properties, the crystal size and the extent of structural disorder. Catalytic activity and selectivity of the *Me*–V–O catalysts decrease in the order Mg > Pb > Zn. The lower activity of Zn–V–O and Pb–V–O catalysts in comparison with Mg–V–O samples of similar composition is assumed to be due to large crystallites with low surface defect concentration.**

Key Words: **metal vanadate catalysts; oxidative dehydrogenation of propane; structure–reactivity relationships;** *in situ* **EPR;** *in situ* **UV/VIS;** *quasi in situ* **XPS.**

INTRODUCTION

The oxidative dehydrogenation (ODH) of lower alkanes to the respective olefins being of high industrial interest has been extensively studied since the 1970s and comprehensively discussed in several review papers (1–3). Nevertheless, in propane ODH, maximum propene yields obtained so far do not markedly exceed 20%. For rational catalyst design, detailed information on the nature of the active sites and their role in the catalytic cycle is needed. However, the current knowledge on these subjects is still incomplete and frequently contradictory.

Mixed oxides based on vanadia and, in particular, Mg–V–O compounds belong to the most effective catalysts for the ODH of propane and have been frequently studied in this reaction (1–11). Generally, vanadium ions are assumed as active sites. However, their structure, in a particular coordination and valence state, are still controversially discussed. Depending on the V/Mg ratio magnesium ortho-, $Mg_3(VO_4)_2$, pyro-, $Mg_2V_2O_7$, and metavanadate, MgV_2O_6, have been observed as crystalline phases besides MgO and V_2O_5 in Mg–V–O materials. Kung and co-workers identified isolated tetrahedral VO_4^{3-} units in Mg orthovanadate to be the active and selective species in the ODH of propane. They explained the higher selectivity of these sites in comparison to dimeric tetrahedral V^{5+} in Mg pyrovanadate by the presence of Mg–O–V units in the former in which the vanadium ions are assumed to be less easily reducible than in V–O–V units in pyrovanadate (4, 5). In contrast, Siew Hew Sam *et al.* regarded α-$Mg_2V_2O_7$ as an active and selective phase and $Mg_3(VO_4)_2$ as responsible for total oxidation (6). High catalytic performance of α-$Mg_2V_2O_7$ has been observed, too, by Guerrero-Ruiz *et al.* who stated that the easier a catalyst is reduced, the higher the propene selectivity (7). However, the opposite relationship has been established by Kung and Kung (8) who correlated dropping ODH selectivities to increasing oxidation potentials of the metal cations in a number of metal orthovanadates. They concluded that the easier it is to reduce the metal vanadate, i.e., to remove lattice oxide ions, the more likely the vanadate will react with the hydrocarbon to result in carbon oxides. Pantazidis *et al.* attributed high catalytic performance to the presence of mixed and inhomogeneous MgO/Mg–V–O phases containing anion vacancies rather than to pure Mg vanadates (9). A synergistic effect on the catalytic performance has also been ascribed to the co-existence of two phases in $MgO/Mg_3(VO_4)_2$ and $Mg_2P_2O_7/Mg_3(VO_4)_2$ biphasic systems, although this phenomenon is not understood up to now (10). In a recent *in situ* study using combined

[1] To whom correspondence should be addressed. Fax: +49 (0) 30 63 92 43 50. E-mail: ab@aca-berlin.de.

0021-9517/01 $35.00

EXAFS/XRD measurements, the formation of a spinel-type phase, MgV_2O_4, with trivalent vanadium has been identified under reaction conditions (11).

The discrepancies in the results obtained by different authors from investigations of similar catalysts might arise from different preparation procedures and conditions of catalytic tests, in particular, different oxygen partial pressures of the feed. Against this background, it is the aim of this work to derive structure–reactivity relationships for metal vanadate catalysts used in the ODH of propane. In particular, it shall be elucidated how coordination, valence state, and redox behavior of the vanadium sites present in different phases influence activity and propene selectivity of the various catalysts. This is done, on the one hand, using a variety of *ex situ* characterization methods and, on the other hand, by monitoring the behavior of the catalysts under reaction conditions using *in situ* EPR, *in situ* UV/VIS, and *quasi in situ* XPS. In comparison to Mg–V–O catalysts used as a model system, the properties of Zn and Pb vanadates have been studied. The structure of the anions and, thus, the vanadium coordination in corresponding vanadate phases of the three different metals is rather similar. However, the redox behavior and the acid–base properties are expected to be different. This provides a good possibility in studying the particular influence of the various metal cations on these properties and, in turn, on the catalytic behavior in the ODH of propane.

METHODS

1. Catalysts

Mg–V–O catalysts were prepared by two different procedures. Samples of Mg/V atomic ratios of 9/1, 4/1, 1/1, and 1/4 were obtained by a precipitation method using NH_4VO_3 and $Mg(OH)_2$ precipitated from a 0.25 M $MgCl_2 \cdot 6H_2O$ by adding 0.5 M KOH (6). The $Mg(OH)_2$ powder was added in portions to an aqueous solution of NH_4VO_3 and 1 wt% of NH_4OH. After evaporation in a rotary evaporator, the resulting powder was dried at 383 K for 18 h and calcined in air at 873 K for 3 h. Samples obtained by this procedure are denoted as Mg_9V_1(p), Mg_4V_1(p), Mg_1V_1(p), and Mg_1V_4(p).

Samples of Mg/V atomic ratios of 3/2, 1/1, and 5/4 were prepared by the citrate method, details of which are described elsewhere (10). Briefly, citric acid was added to a transparent aqueous solution containing appropriate amounts of $Mg(NO_3)_2$ and NH_4VO_3. After evaporation, the resulting precursor was decomposed in air at 653 K for 18 h and finally calcined in air at 873 K for 3 h. Catalysts prepared by this method are denoted as Mg_3V_2(c), Mg_1V_1(c), and Mg_5V_4(c).

Zn vanadate catalysts of Zn/V atomic ratios of 3/2 (Zn_3V_2), 1/1 (Zn_1V_1), and 5/4 (Zn_5V_4) were prepared by adding an appropriate amount of $ZnCO_3$ powder to a hot aqueous solution of NH_4VO_3. After evaporation in a rotary evaporator, the resulting powder was dried at 383 K for 18 h and calcined in air at 873 K for 3 h.

Pb vanadate catalysts of Pb/V atomic ratios 3/2 (Pb_3V_2), 1/1 (Pb_1V_1), and 5/4 (Pb_5V_4) were prepared by adding appropriate amounts of solid Pb acetate in portions to a hot aqueous solution of NH_4VO_3. After evaporation in a rotary evaporator, the resulting powder was dried at 383 K for 12 h and calcined in air at 873 K for 3 h.

The BET surface area of the catalysts was determined by N_2 adsorption at 77 K using a Gemini III 2375 surface area analyzer (Micromeritics). The vanadium valence state was determined by potentiometric titration using a variant of the method developed by Niwa and Murakami (12).

2. Catalyst Characterization

EPR spectra were recorded by the c.w. spectrometer ELEXSYS 500-10/12 (Bruker) in X-band. *In situ* investigations under catalytic reaction conditions were performed using a homemade flow reactor equipped with a temperature programmer and connected to a gas dosing apparatus (13, 14). In each run 100 mg of catalyst particles (0.31–0.63 mm) were treated with a total gas flow of 3.6 L h^{-1} consisting of 13.5 mol% C_3H_8/6.8 mol% O_2/N_2 at 773 K (Mg–V–O) or 823 K (Zn–V–O, Pb–V–O). For on-line product analysis the reactor outlet was connected to a GC 17AAF capillary gas chromatograph (Shimadzu) equipped with a 30 m × 0.32 mm Silicaplot column (Chrompack) and a FID.

The spin concentration of EPR-active V^{4+} was determined by comparing the intensities of the EPR signals (double integrals) of the catalysts measured at room temperature with that of a $VOSO_4$ standard prepared by diluting $VOSO_4 \cdot 3\ H_2O$ with K_2SO_4 (15). As indicated by potentiometric titration (12), the standard contained 3.97×10^{20} spins g^{-1}. EPR measurements of sample and standard were performed using the Bruker X-band double-cavity ER 4105 DR.

The X-ray photoelectron spectra were recorded using a VG ESCALAB 220 iXL spectrometer (VG Instruments) at room temperature with a monochromated Al$K\alpha$ source. Charging effects at insulators were reduced by a flood gun. The spectra were corrected with respect to the C 1*s* signal at 284.5 eV. Signal intensities were normalized using the sensitivity factors of Scofield (16) and the transmission function of the spectrometer. In certain cases, spectra were recorded after treating the catalysts in a flow of 13.5 mol% C_3H_8/6.8 mol% O_2/N_2 at 773 K using a reaction cell installed in the lock to the analysis chamber. After subsequent cooling to room temperature, the samples were transferred into the analysis chamber of the spectrometer without contact to ambient atmosphere. In due course XPS measurements performed in this way are labeled "*quasi in situ*."

UV/VIS-DRS measurements were performed using a Cary 400 UV/VIS spectrometer (Varian) equipped with a diffuse reflectance accessory (praying mantis, Harrick). To reduce light absorption, the catalysts were diluted with $BaSO_4$ (Merck, white standard). For *in situ* measurements under reaction conditions, the diffuse reflectance accessory was equipped with a heatable reaction chamber (Harrick). In these cases α-Al_2O_3 (calcined at 1473 K for 4 h) was used as dilution material. A flow of 13.5 mol% C_3H_8/6.8 mol% O_2/N_2 was passed through the catalyst bed.

SEM micrographs were obtained by means of a Amray 1000B microscope (KYKY). Samples were deposited on a metal disc and made conductive with gold using a MED 020 Coating System (BAL-TEC). TEM micrographs were recorded at an acceleration voltage of 200 kV using a CM20 microscope (Philips). Samples were deposited on Lacey carbon film on copper grids. EDX analysis was performed using a PV 9900 spectrometer (EDAX). XRD powder patterns were recorded using a STADI P transmission diffractometer (STOE) using Cu$K\alpha$ radiation at room temperature.

Acidic surface sites were determined by pyridine adsorption using a FTIR spectrometer (Bruker IFS 66) equipped with a heatable adsorption cell. Self-supporting wafers were pretreated in vacuum at 673 K. FTIR spectra were recorded after pyridine adsorption at room temperature and subsequent evacuation. Additionally, surface acidity was evaluated by temperature-programmed desorption of ammonia (TPDA) since, in the case of Zn vanadates, it was not possible to obtain self-supporting wafers from these materials. Samples of 0.8–1.0 g saturated with CO_2 during their storage in air were loaded with ammonia at 373 K for 0.5 h using a 3 vol% NH_3/He flow (90 ml/min). After being flushed with He (50 ml/min) at 373 K for 1 h, the samples were heated at 5 K/min to 873 K in He flow. Desorption/reaction of ammonia as well as the desorption of carbon dioxide were followed using the multi-ion-detection mode of the mass spectrometer QMG 420C (Balzers) by monitoring the ion current profiles at $m/z = 2$ (H_2^+), $m/z = 14$ (N^+ from NH_3 and N_2), $m/z = 15$ (NH^+ from NH_3), $m/z = 28$ (N_2^+, CO^+ from N_2 and CO_2, respectively), $m/z = 44$ (CO_2^+ from CO_2, N_2O^+ from N_2O), $m/z = 30$ (NO^+ from NO), and $m/z = 46$ (NO_2^+ from NO_2). N_2 pulses (500 μl) were used to calibrate the peak areas considering the different ionization probabilities and relative ion currents of the fragments.

TPR measurements were performed by heating samples of about 20 mg at 10 K/min up to 1173 K in a 5 vol% H_2/Ar flow (40 ml/min) and holding 0.5 h. The formed water was removed from the H_2/Ar flow by trapping with molecular sieve 4A. Changes in the H_2 concentration were measured by a thermal conductivity detector (TCD). The areas of the TPR peaks were calibrated by Ar pulses (500 μl) into the H_2/Ar flow. To compare the reducibility of the catalysts, the temperature of the onset of the hydrogen consumption (T_{onset}) was used. This parameter was defined as the temperature of the 5% increase of the TCD signal compared to the maximum of the TPR peak.

3. *Catalytic Tests*

Catalytic tests were performed at atmospheric pressure in a fixed-bed U-type quartz reactor (internal diameter 4 mm) at 773 K (Mg–V–O) or 823 K (Zn–V–O, Pb–V–O) using an educt mixture of 40 vol% C_3H_8/20 vol% O_2/N_2. The total flow rate was varied between 10 and 100 ml min^{-1}. The sample particles (250–380 μm) were diluted with quartz particles in a ratio of 1 : 5. The catalyst mass was 0.05 g (Mg–V–O) and 0.15–0.3 g (Zn–V–O and Pb–V–O). The reaction products were analyzed by on-line gas chromatography using a Satochrom gas chromatograph. A molecular sieve 5A column and a thermal conductivity detector were used to determine the content of O_2, N_2, and carbon oxides while the hydrocarbons were analyzed on a Poraplot-Q capillary column using a flame ionisation detector.

RESULTS AND DISCUSSION

1. *Phase Composition and Surface Properties*

Phase composition and particle size. Depending on the Mg/V atomic ratio in the synthesis mixture, different crystalline phases are observed by XRD in Mg–V–O catalysts (Table 1). MgO is formed as a major component in Mg_9V_1(p) or as a minor component besides magnesium orthovanadate in Mg_4V_1(p) when magnesium is in excess. Stoichiometric Mg/V atomic ratios lead to the crystallization of magnesium ortho- and/or pyrovanadate while an excess of vanadium in the synthesis mixture gives rise to V_2O_5 as a major phase in addition to a small amount of magnesium metavanadate. TEM micrographs indicate that crystallites of Mg–V–O samples prepared by precipitation (15–50 nm) are smaller than those of catalysts obtained by the citrate method (30–200 nm) (Figs. 1a and 1b), which might give rise to the stronger XRD reflections of the latter. EDX analysis of the Mg–V–O crystallites revealed that their composition is rather homogeneous corresponding virtually to the Mg/V atomic ratios in the synthesis mixtures.

Zn–V–O catalysts with the same metal/V atomic ratio contain crystalline phases similar to those of the respective Mg–V–O samples (Table 1). However, in contrast to the latter, XRD reflections of Zn–V–O samples are about six times more intense, probably due to the much larger crystallites ($\approx$1 μm) as confirmed by TEM micrographs (Fig. 1c).

In Pb–V–O catalysts, crystalline ortho- and pyrovanadates of lead have been detected, too, by XRD (Table 1). However, the preparation method does obviously not provide as good control of phase composition as was observed with Mg–V–O and Zn–V–O catalysts. While lead orthovanadate is the only detectable crystalline phase for atomic

TABLE 1

Crystalline Phases, Content of Total and Reduced Vanadium, Mean Vanadium Valence State, and BET Surface Area of the Catalysts

Sample	Crystalline phases (XRD)	Total V/at%[a]	S_{BET}/m^2 g^{-1}	Mean V valence[a]	V^{4+}/at%[a]	V^{4+}/at%[b]
Mg_9V_1(p)	MgO, $Mg_3V_2O_8$	4.7	87.4	4.68	1.5	0.08
Mg_4V_1(p)	$Mg_3V_2O_8$, MgO	8.75	46.9	4.86	1.2	0.06
Mg_3V_2(c)	$Mg_3V_2O_8$	15.5	21.6	4.90	1.6	—
Mg_5V_4(c)	$Mg_3V_2O_8$, $Mg_2V_2O_7$	16.8	17.7	4.92	1.3	—
Mg_1V_1(c)	$Mg_2V_2O_7$	18.4	9.5	4.87	2.4	—
Mg_1V_1(p)	$Mg_2V_2O_7$	18.3	7.9	4.91	1.7	—
M_1V_4(p)	V_2O_5, MgV_2O_6	25.3	1.9	4.92	2.1	0.09
Zn_3V_2	$Zn_3V_2O_8$	15.5	1.6	4.89	1.6	—
Zn_5V_4	$Zn_2V_2O_7$, $Zn_3V_2O_8$	16.8	0.7	4.91	1.5	—
Zn_1V_1	$Zn_2V_2O_7$	18.3	1.0	4.92	1.5	—
Pb_3V_2	$Pb_3V_2O_8$	15.9	0.3	4.57	6.8	—
Pb_5V_4	$Pb_3V_2O_8$	17.1	0.32	4.71	4.9	—
Pb_1V_1	$Pb_2V_2O_7$, $Pb_3V_2O_8$	18.55	1.2	4.78	4.0	—

[a] Determined by potentiometric titration.
[b] Derived from determination of spin concentration using EPR.

ratios of Pb/V = 3/2 and 5/4, a mixture of ortho- and pyrovanadate is obtained with a ratio of Pb/V = 1/1. The XRD reflections of Pb vanadate phases are less intense than those of Mg vanadates. Unfortunately, no information on the structure of the crystallites is available since the TEM microcraphs are only poorly resolved due to the strong absorption of lead.

Reducibility. In all as-synthesized catalysts a certain percentage of tetravalent vanadium has been detected by potentiometric titration (Table 1). Within each group of metal/vanadium oxides the V^{4+} content increases with rising metal/V atomic ratio. In as-synthesized Mg–V–O catalysts the mean V valence is lowest for sample Mg_9V_1(p). Pb–V–O catalysts are markedly more reduced than the corresponding Mg–V–O and Zn–V–O samples. It seems rather unlikely that crystalline $Pb_2V_2O_7$ and $Pb_3V_2O_8$ can accommodate such large amounts of tetravalent vanadium without degradation of the crystal structure. This suggests the presence of additional amorphous components containing mainly tetravalent vanadium, which could be the reason for the lower intensity of the XRD reflections in comparison to those of Zn–V–O and Mg–V–O samples.

In the TPR profiles, T_{onset} is shifted to higher temperatures with decreasing metal/vanadium ratio (Figs. 2 and 3). The stepwise reduction of V_2O_5 via V_6O_{13}, V_2O_4, to V_2O_3 (17) dominates the TPR profile of the Mg_1V_4(p) sample, which agrees well with XRD and TEM results showing the presence of an excess of V_2O_5 in this sample. The profiles of Pb–V–O catalysts show shoulders on the high-temperature flank of the peaks of the respective Pb vanadates. The rather high V^{4+} content (Table 1) suggests the presence of additional amorphous phases, which could be one reason for the asymmetric TPR profile. Moreover, the difference between the experimental and calculated H_2 consumptions (Table 2) indicates that in addition to the reduction of V^{5+} and V^{4+} to V^{3+}, Pb^{2+} is also reduced to Pb^0. In the case of the zinc vanadates, Zn^{2+} is at least partially reduced because a gray deposition of metallic zinc was observed at the cold reactor outlet. However, this effect seems to play only a minor role, as can be seen from the H_2 consumption values in Table 2.

Surface composition. XPS data of as-synthesized catalysts are summarized in Table 3. The metal/vanadium atomic ratios on the surface are similar to those derived from the bulk composition, pointing to a rather homogeneous elemental distribution in the whole samples. This is in agreement with the EDX results. In magnesium and zinc vanadate samples with metal/vanadium molecular ratios of

TABLE 2

TPR Results

Sample	H_2 consumption/mmol g^{-1}		T_{onset}/K
	Calculated[a]	Experimental	
Mg_9V_1(p)	1.90	1.67	750
Mg_4V_1(p)	3.65	3.49	813
Mg_3V_2(c)	6.10	5.93	829
Mg_5V_4(c)	6.74	6.46	821
Mg_1V_1(c)	6.99	7.15	823
Mg_1V_1(p)	7.33	7.09	832
Mg_1V_4(p)	9.46	9.04	879
Zn_3V_2	4.39	4.01	781
Zn_5V_4	5.09	5.10	785
Zn_1V_1	5.38	5.36	813
Pb_3V_2	1.79	5.53	827
Pb_5V_4	1.52	5.13	831
Pb_1V_1	2.59	5.90	845

[a] Calculated assuming that all V^{5+} and V^{4+} determined by potentiometric titration (Table 1) is reduced to V^{3+}.

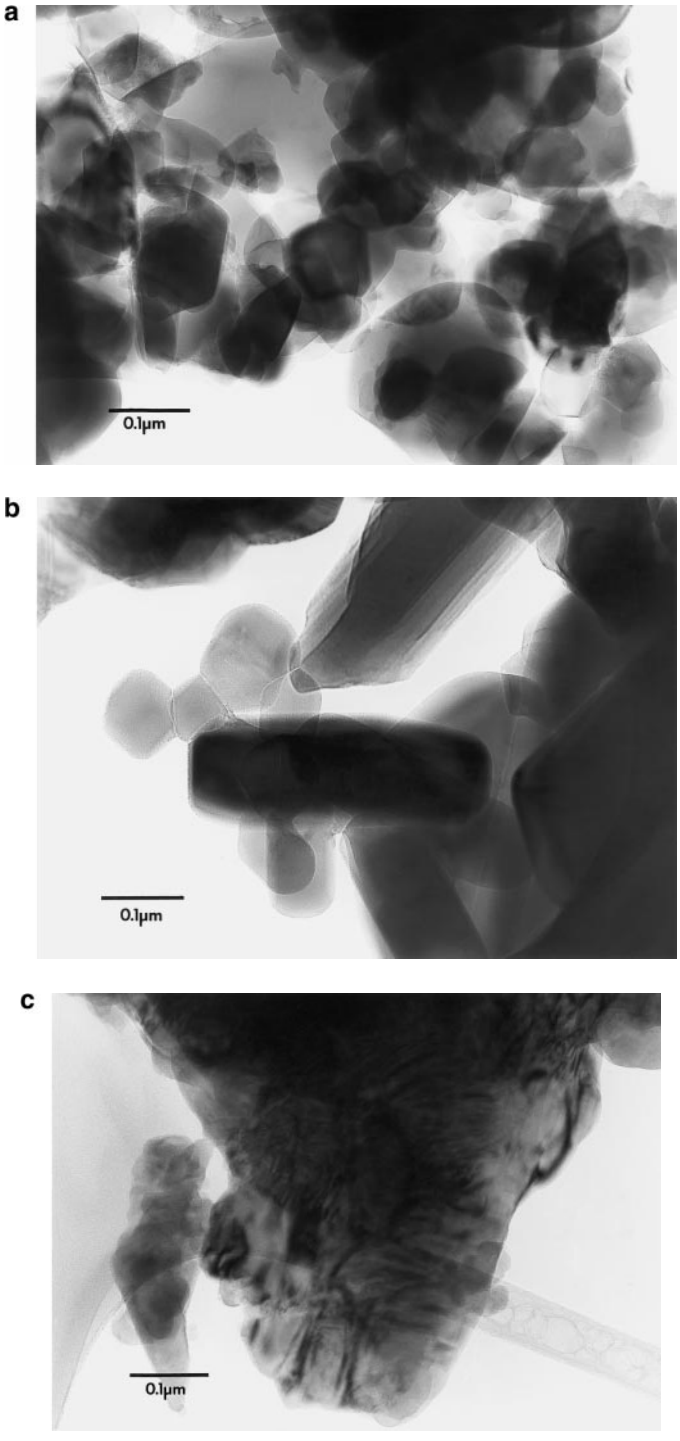

FIG. 1. TEM micrographs of (a) sample Mg_1V_1(p), (b) sample Mg_1V_1(c), and (c) sample Zn_1V_1.

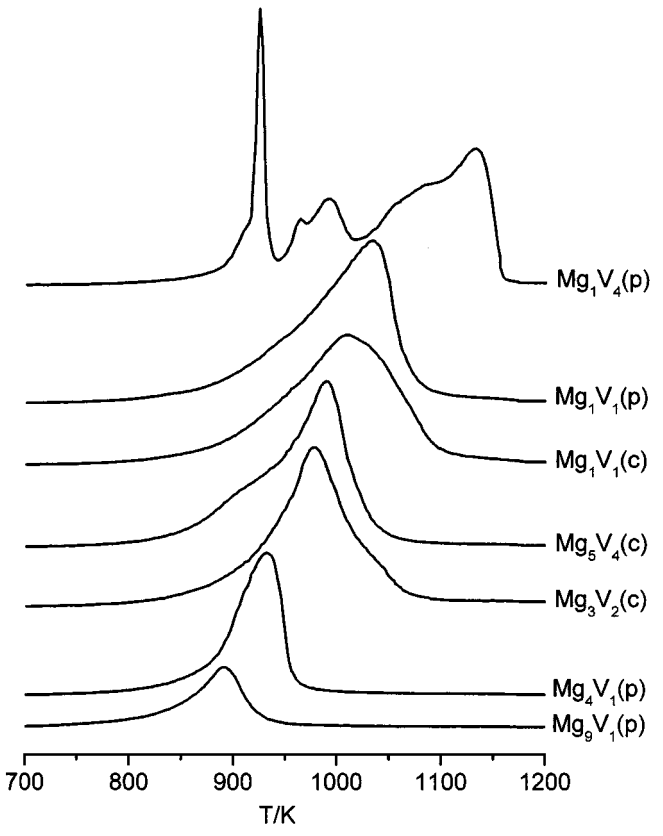

FIG. 2. TPR profiles of Mg–V–O samples.

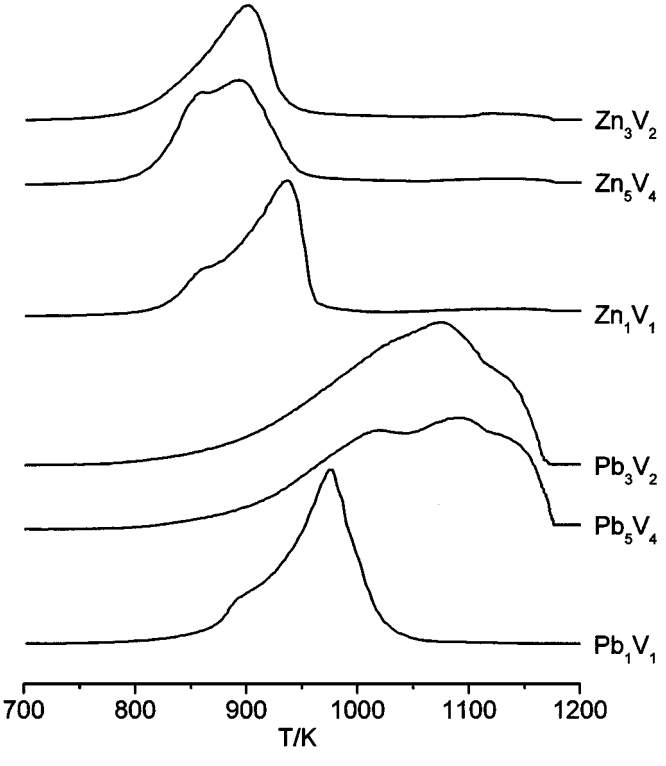

FIG. 3. TPR profiles of Zn–V–O and Pb–V–O samples.

1/1, 3/2, and 5/4 only pentavalent vanadium represented by V $2p_{3/2}$ binding energies between 518.6 and 519.9 eV has been detected on the surface, although the mean vanadium valence state is slightly less than +5 (Table 1). A reason may be that V^{4+} is readily oxidized on the surface of these samples upon contact with air. The V $2p_{3/2}$ binding

TABLE 3

Binding Energies, E_B, and Surface Content for Catalyst Constituents Derived by XPS

Sample	Signal	E_B/eV	Content/at%[a]	Sample	Signal	E_B/eV	Content/at%[a]
Mg_9V_1(p)	O 1*s*	529.6	60.3	Mg_1V_4(p)	O 1*s*	530.2	61.7
	V $2p_{3/2}$	517.0	1.9		V $2p_{3/2}$	517.4	19.6
		514.9	1.3		Mg 2*p*	50.1	3.6
	Mg 2*p*	46.7	29.7				
Mg_4V_1(p)	O 1*s*	529.6	58.1	Mg_1V_4(p)[b]	O 1*s*	529.9	78.7
	V $2p_{3/2}$	517.1	3.1		V $2p_{3/2}$	516.9	7.5
		515.4	2.5			515.4	9.2
	Mg 2*p*	46.8	25.8		Mg 2*p*	49.5	4.6
Mg_3V_2(c)	O 1*s*	532.6	50.7	Zn_3V_2	O 1*s*	532.7	48.3
	V $2p_{3/2}$	519.8	10.2		V $2p_{3/2}$	519.6	6.0
	Mg 2*p*	51.9	19.4		Zn $2p_{3/2}$	1024.2	10.8
Mg_5V_4(c)	O 1*s*	532.6	49.7	Zn_5V_4	O 1*s*	532.6	52.9
	V $2p_{3/2}$	519.9	10.5		V $2p_{3/2}$	519.7	7.9
	Mg 2*p*	52.0	16.9		Zn $2p_{3/2}$	1024.2	8.7
Mg_1V_1(c)	O 1*s*	532.4	51.3	Zn_1V_1	O 1*s*	532.5	39.7
	V $2p_{3/2}$	519.8	8.4		V $2p_{3/2}$	519.8	3.6
	Mg 2*p*	52.0	10.3		Zn $2p_{3/2}$	1024.3	5.0
Mg_1V_1(c)[b]	O 1*s*	532.5	57.2	Pb_3V_2	O 1*s*	529.0	43.3
	V $2p_{3/2}$	519.8	11.4			530.1	12.3
		517.9	8.6		V $2p_{3/2}$	515.7	11.0
	Mg 2*p*	52.9	18.2			516.6	2.8
					Pb 4 $f_{7/2}$	137.6	18.0
Mg_1V_1(p)	O 1*s*	531.6	42.5	Pb_5V_4	O 1*s*	528.0	53.3
	V $2p_{3/2}$	518.6	10.0		V $2p_{3/2}$	513.4	4.0
	Mg 2*p*	51.0	12.2			514.9	8.6
					Pb 4 $f_{7/2}$	138.4	17.2
				Pb_1V_1	O1*s*	528.3	19.6
						529.4	36.7
					V $2p_{3/2}$	515.6	13.3
					Pb 4 $f_{7/2}$	137.8	14.0

[a] Difference to 100% due to carbon impurities.
[b] *Quasi in situ* XPS data after treatment under propane ODH conditions.

energies in these vanadates are higher than the value expected for pure V_2O_5 (517.4 eV (18)). This trend was observed by other authors, too, and has been explained in terms of increasing ionic character of the V–O bond in the vanadates (6). In sample M_1V_4(p), which contains V_2O_5 as a separate phase, the V $2p_{3/2}$ peak occurs at 517.4 eV, which is very close to the value determined for pure V_2O_5 (18). When the mean vanadium valence decreases as in the case of samples M_9V_1(p) and M_4V_1(p), a certain percentage of reduced vanadium (E_B = 514.9 and 515.3 eV, Table 3) is also detected on the surface. The same holds for Pb–V–O samples, showing a rather low mean vanadium valence (Table 1). In general, the V $2p_{3/2}$ peak in these samples appears at rather low binding energies. Based on a comparison with pure vanadium oxides, values of 515.6 and 515.7 eV should be assigned to V^{3+} and 516.6 eV to V^{4+} (18). However, this would mean that the surface of lead vanadates should be markedly more reduced than the bulk, which seems to be improbable since the samples were stored in air. Alternatively, the shift to lower binding energies could be caused by the presence of the heavy lead ion. A similar shift of the V $2p_{3/2}$ peak is observed, too, within the group of alkali vanadates from Li_3VO_4 (517.5 eV) to Cs_3VO_4 (516.9 eV) (18). With respect to this consideration we attribute the V $2p_{3/2}$ peaks at 515.6 and 515.7 eV to V^{4+} and the one at 516.6 eV to V^{5+}. In sample Pb_5V_4 partial charging effects cannot be excluded, which could be the reason for the unusually low V $2p_{3/2}$ binding energies (Table 3). Such effects might also be responsible for the deviations of the binding energy observed for Mg in samples Mg_9V_1(p) and Mg_4V_1(p) and for V and Zn in Zn–V–O catalysts. They can be compensated for by depositing conducting gold particles of ≈20 nm in size as a reference on the samples (19). This has been done for samples Mg_4V_1 and Zn_5V_4. Under these conditions the peaks in Mg_4V_1 occur at 531.7 eV (O 1*s*), 517.3 eV (V $2p_{3/2}$), and 49.7 eV (Mg 2*p*) and in Zn_5V_4 at 530.2 eV (O 1*s*), 517.1 eV (V $2p_{3/2}$), and 1021.6 eV (Zn $2p_{3/2}$).

Acid–base properties. Acid–base properties of the catalyst surface have been studied by FTIR spectroscopy using pyridine adsorption and by temperature-programmed desorption of ammonia (TPDA). In all Mg–V–O catalysts Lewis surface sites evidenced by a FTIR band around 1440 cm^{-1} were detected. The band area normalized on the BET surface area of the catalysts rises with increasing vanadium content (arbitrary units): Mg_9V_1(p): 4.6 < Mg_3V_2(c): 7.4 < Mg_5V_4(c): 11.9 ≈ Mg_1V_1(c): 10.5 < Mg_1V_4(p): 26.3. This indicates that Lewis acidity is related to the vanadium surface sites. The band position is slightly shifted to higher wavelengths in the order Mg_3V_2(c) < Mg_9V_1(p) < Mg_5V_4(c) < Mg_1V_1(c) < Mg_1V_4(p), pointing to increasing strength of the Lewis sites (20). Despite sample Mg_1V_4(p) in which a weak band at 1536 cm^{-1} arises from pyridine adsorbed at Brønsted sites, no such sites have been detected in all other Mg–V–O catalysts. On the surface of Pb–V–O catalysts no pyridine adsorption could be detected by FTIR, indicating the absence of both Lewis and Brønsted sites. Since Zn–V–O catalysts could not be pressed into self-supporting discs, the surface acidity of Zn_1V_1 has been studied by TPDA in comparison to that of Mg_1V_1(c).

TPD/TPRS profiles of the samples Mg_1V_1(c) and Zn_1V_1 are shown in Fig. 4. The ion current profiles $m/z = 15$ and 14 reveal the desorption of weakly bound ammonia between 400 and 700 K for both samples. However, a considerable part of NH_3 is so strongly bound that it does not reversibly desorb but is oxidized to nitrogen as indicated by comparable shapes and peak maxima of the $m/z = 28$ and $m/z = 14$ profiles at ca. 700 K (Mg_1V_1(c)) and 670 K (Zn_1V_1). NO or NO_2 were observed in traces only. Obviously, the catalysts contain both weak and strong acidic sites, the latter fixating ammonia molecules on the surface until their oxidation at higher temperatures.

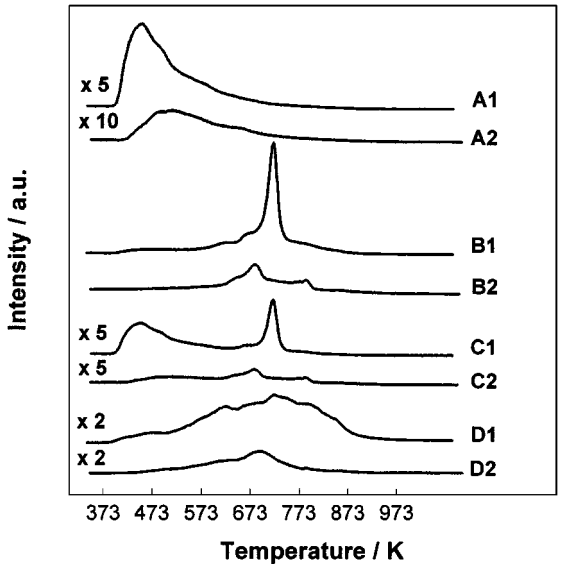

FIG. 4. Ion current profiles of temperature-programmed desorption/reaction of carbon dioxide and ammonia from catalyst Mg_1V_1(c) (1) and Zn_1V_1 (2), $m/z = 15$ (A), $m/z = 28$ (B), $m/z = 14$ (C), and $m/z = 44$ (D).

Apart from the desorption of ammonia and nitrogen, the desorption of carbon dioxide can be observed. The $m/z = 44$ profiles of both samples show a peak with a shoulder on its low-temperature flank, pointing to basic sites of different strength. The profile $m/z = 44$ can be clearly attributed to CO_2 because N_2O can be excluded due to the noncorresponding shapes and intensities of the $m/z = 30$ profile (NO^+ from N_2O). Furthermore, shoulders observed on both flanks of the $m/z = 28$ peaks cannot be related to CO_2 desorption (CO^+ fragments) because of the same shape of the $m/z = 14$ and $m/z = 28$ profile in this range.

The total amount of adsorbed ammonia, i.e., the total amount of acidic sites, was calculated from the ammonia and nitrogen desorption (Table 4). The amount of the basic sites, i.e., the amount of desorbed CO_2, is rather low with respect to that of acidic sites. However, it has to be considered that CO_2 was adsorbed during storage in air, i.e., in competition with water vapor. The basicity of these sites is rather high since the major part of CO_2 desorbs only between 573 and 873 K. Upon comparison of the surface area of specific amounts of desorbed NH_3 and CO_2, it is readily seen that the concentration of both acidic and basic sites is markedly higher for sample Zn_1V_1 than for Mg_1V_1(c). This holds in particular for strong acidic sites comprised by the amount of formed N_2. In contrast, the strength of acidic and basic sites is virtually similar for both samples. From the described investigations it turns out that the concentration of acidic sites on the surface of metal vanadates increases in the order 0 ≈ Pb–V–O ≪ Mg–V–O < Zn–V–O.

2. *Structure of Vanadium Sites*

The catalysts have been studied by EPR and UV/VIS-DRS spectroscopy being complementary methods to obtain information on the local coordination geometry of VO_x species. By EPR, only V^{4+} in distorted octahedral or square pyramidal symmetry can be observed at temperatures higher than 77 K while V^{3+} and V^{4+} in tetrahedral symmetry are not detected due to very short relaxation times [20]. In contrast, UV/VIS spectra show intense charge-transfer (CT) bands for V^{5+} while V^{4+} and V^{3+} are hardly detectable especially in the presence of V^{5+} as major component.

UV/VIS–DRS measurements. The UV/VIS spectrum of sample Mg_3V_2(c) shows three bands at 218, 280, and 341 nm (Fig. 5), which can be assigned to CT transitions of isolated tetrahedrally coordinated V^{5+} (21). This is in agreement with the crystal structure of $Mg_3(VO_4)_2$ (6) being the main phase of this catalyst. In sample Mg_1V_1(c), CT bands are red-shifted to 225, 300, and 370 nm being characteristic of $V^{5+}O_4$ tetrahedra connected via V–O–V bonds (22). This agrees well with the fact that the main phase

TABLE 4

Evaluation of the Peak Areas of the TPD/TPRS Measurements

Sample	NH_3 adsorbed/μmol m^{-2}	NH_3 desorbed/μmol m^{-2}	N_2 formed/μmol m^{-2}	CO_2 desorbed/μmol m^{-2}
Mg_1V_1(c)	27.6	20.6	3.5	2.9
Zn_1V_1	85.0	51.0	17.0	9.0

of Mg_1V_1(c) is $Mg_2V_2O_7$, the crystal structure of which contains dimers of VO_4 tetrahedra (2). The spectrum of sample Mg_1V_4(p) contains bands at 290, 311, 394, and 480 nm, which can be assigned to CT transitions of crystalline V_2O_5, being the main component of this catalyst (22). Additionally, the catalyst contains a small amount of MgV_2O_6, which forms chains of VO_6 octahedra (4). Their CT bands have positions similar to those of V_2O_5 except the band at 480 nm, which is characteristic only for crystalline V_2O_5 (22). In samples Mg_9V_1(p) and Mg_4V_1(p) weak bands at 380 and 386 nm are observed in addition to those arising from $Mg_3(VO_4)_2$. They indicate the presence of oligomeric tetrahedrally and probably some octahedrally coordinated V^{5+}.

The UV/VIS bands for Zn_1V_1 and Zn_5V_4 catalysts (Fig. 6) fall at similar wavelengths as in Mg_1V_1(c) due to the fact that $Zn_2V_2O_7$ is the main component of these samples containing dimers of VO_4 tetrahedra like $Mg_2V_2O_7$. In the spectrum of sample Zn_3V_2 containing crystalline $Zn_3(VO_4)_2$ with isolated VO_4 tetrahedra as the main component, the CT band at lowest energy is blue shifted and less intense, suggesting only a minor however not negligible influence of connected VO_4 tetrahedra.

The UV/VIS spectra of the Pb–V–O catalyst are rather similar to those of the respective Zn–V–O samples (Fig. 6) since the local structure of the vanadium ions (VO_4^{3-} and $V_2O_7^{4-}$) in the crystalline Pb vanadates is the same as that in the corresponding Zn vanadates. However, the Pb–V–O samples show a slightly higher absorption in the wavelength range below 300 nm in which the CT bands of V^{4+} are expected (21, 24). This could be due to the rather high V^{4+} content (Table 1). Moreover, the lowest energy CT band in samples Pb_3V_2 and Pb_5V_4 containing Pb orthovanadate with isolated VO_4 units as the only crystalline phase falls at 368 nm. This indicates the presence of some connected VO_4 species probably within an additional amorphous component discussed above.

EPR measurements. In the EPR spectra of Mg–V–O catalysts, a signal with hyperfine structure (hfs) being

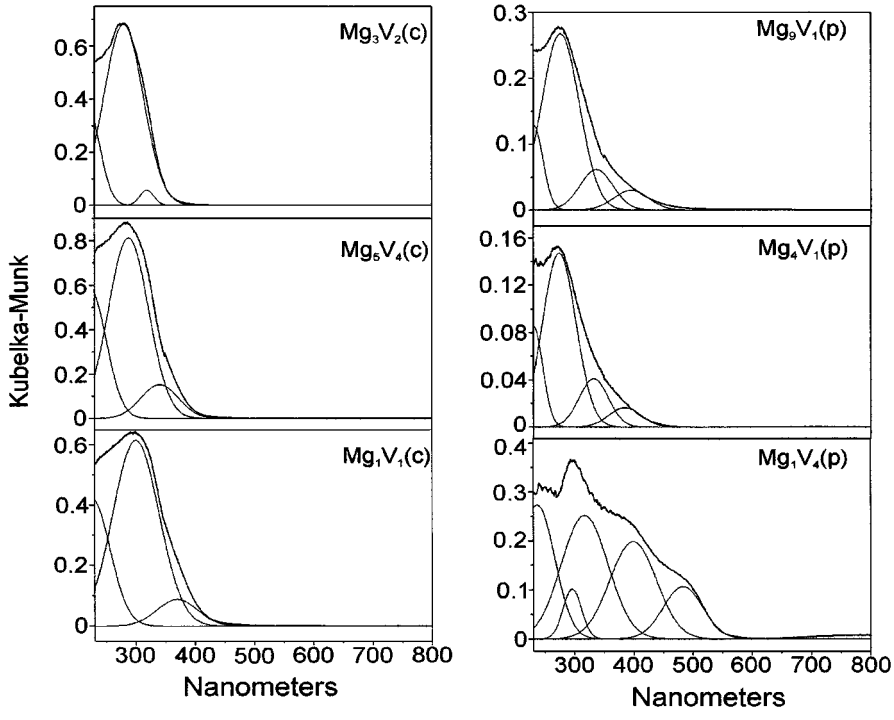

FIG. 5. UV/VIS-DRS spectra of as-synthesized Mg–V–O catalysts at room temperature; thick line, experimental, thin lines, deconvoluted bands.

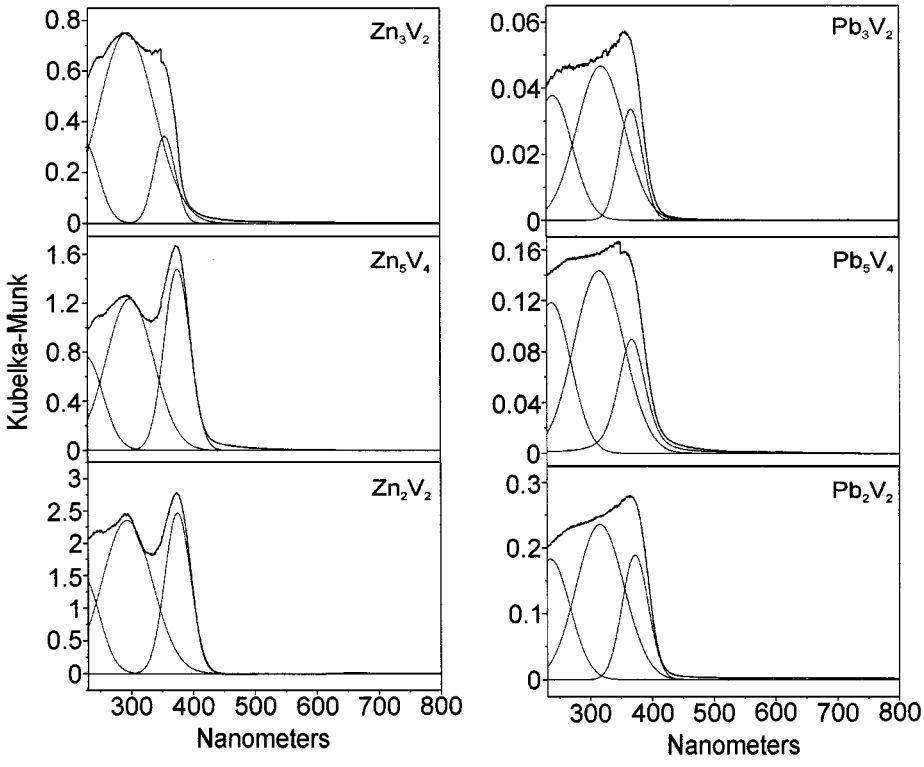

FIG. 6. UV/VIS-DRS spectra of as-synthesized Zn–V–O and Pb–V–O catalysts at room temperature; thick line, experimental; thin lines, deconvoluted bands.

characteristic of isolated, axially distorted VO^{2+} ions in square pyramidal or octahedral coordination is superimposed on a broad more or less isotropic singlet arising from weakly interacting VO^{2+} species (Fig. 7). An exception is sample $Mg_1V_4(p)$, which shows a narrow singlet being due to closely neighboring VO^{2+} species coupled by effective spin–spin exchange interactions. Since sample $Mg_1V_4(p)$ contains crystalline V_2O_5, it is very probable that the VO^{2+} clusters are formed by partial reduction of V_2O_5, being a frequently observed phenomenon in this material (24). The values of $g_{\|} = 1.943$, $g_{\perp} = 1.955$, $A_{\|} = 17.1$ mT, and $A_{\perp} = 5.0$ mT derived by spectra simulation from the hfs spectra of samples $Mg_9V_1(p)$ and $Mg_4V_1(p)$ containing MgO as a separate phase are similar to those observed for VO^{2+} in V_2O_5/MgO catalysts ($g_{\|} = 1.949$, $g_{\perp} = 1.959$, $A_{\|} = 17.7$ mT, and $A_{\perp} = 4.8$ mT (25). Thus, it seems likely that in samples $Mg_9V_1(p)$ and $Mg_4V_1(p)$ some VO^{2+} ions are located on octahedral Mg lattice positions in the MgO phase or incorporated in an amorphous vanadia overlayer. Scattering of such an overlayer over the surface of MgO has been detected, too, by Pantazidis *et al.* in a Mg_7V_1 catalyst prepared in a way similar to sample $Mg_9V_1(p)$ (26). The formation of such an amorphous oligomeric VO_x component is also suggested in the UV/VIS results described above.

In samples $Mg_9V_1(p)$ and $Mg_4V_1(p)$, a certain percentage of the V^{5+} species is also in square pyramidal or octahedral coordination, as indicated by the position of the lowest energy CT band in the UV/VIS spectra (Fig. 5). This seems not to be the case for samples $Mg_1V_1(p)$, $Mg_1V_1(c)$, $Mg_5V_4(c)$, and $Mg_3V_2(c)$ consisting of vanadate phases with tetrahedral V^{5+} species (Fig. 5). Accordingly, the EPR signal of VO^{2+} species supposed to be formed by partial reduction of VO^{3+} is markedly smaller than that in the spectra of $Mg_9V_1(p)$, $Mg_4V_1(p)$, and $Mg_1V_4(p)$ (Fig. 7). Partial reduction, which is evident also in samples $Mg_1V_1(p)$, $Mg_1V_1(c)$, $Mg_5V_4(c)$, and $Mg_3V_2(c)$ (Table 1), leads probably mainly to tetrahedral V^{4+}, which is not EPR active due to short relaxation times. This is most obvious for the Pb–V–O catalysts and for sample Zn_3V_2 (pure Zn orthovanadate) for which the EPR signal is too weak to be properly detected. The other two Zn vanadates show only a very small signal resulting mainly from interacting VO^{2+} species.

Upon comparison of the V^{4+} content derived by potentiometric titration with that resulting from the determination of the spin concentration using EPR (Table 1), it is readily evident, even for samples $Mg_1V_4(p)$, $Mg_4V_1(p)$, and $Mg_9V_1(p)$, which show rather strong EPR signals (Fig. 7), that the former value is much higher, indicating that a considerable part of the tetravalent vanadium is EPR silent. In all other samples the EPR signal is too weak to obtain proper double integrals. Besides the tetrahedral coordination discussed above, strong line broadening due to weak magnetic dipolar interactions between less closely

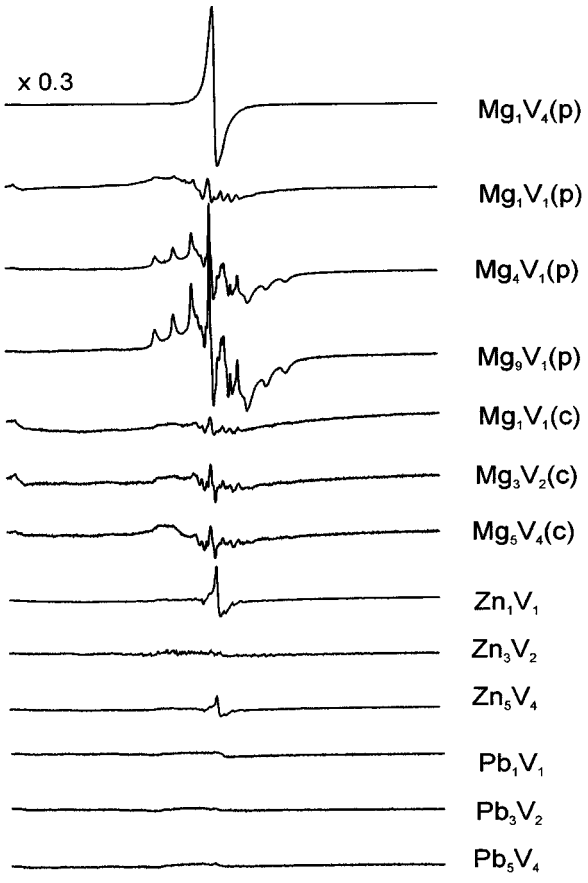

FIG. 7. EPR spectra of as-synthesized catalysts at room temperature in the range $150 < B_0/\mathrm{mT} < 550$.

neighboring VO^{2+} species could be another reason for this result.

3. Structural Changes under Reaction Conditions

To elucidate whether the structure and valence state of the active vanadium sites are modified during propane ODH, samples $Mg_1V_4(p)$ and $Mg_1V_1(c)$ have been studied by *in situ* EPR, *in situ* UV/VIS-DRS, and *quasi in situ* XPS. Upon heating of sample $Mg_1V_4(p)$ under feed at 773 K, the EPR singlet of magnetically interacting VO^{2+} species being present already in the fresh catalyst increases strongly (Fig. 8). This indicates that the V_2O_5 phase contained in this sample is markedly reduced under ODH conditions. This is also confirmed by a decrease of the mean vanadium valence state determined by potentiometric titration from 4.918 in the fresh catalyst to 4.604 after the catalytic test. Indeed, crystalline VO_2 has been detected in the XRD powder pattern of the used catalyst while the reflections of V_2O_5 roughly disappeared. Interestingly, this reduction goes along with an improvement of the catalytic performance (Fig. 8). *Quasi in situ* XPS measurements after pretreatment of sample $Mg_1V_4(p)$ under ODH conditions indicate that 55% of the surface V^{5+} sites are reduced to V^{4+} (Table 3). *In situ* UV/VIS measurements of sample $Mg_1V_4(p)$ during heating in nitrogen flow show a decrease of CT bands around 400 and 480 nm, being characteristic of crystalline V_2O_5 (23) (Fig. 9a). Simultaneously, absorption increases below 250 nm in the range of CT bands of tetravalent vanadium and above 600 nm where d–d bands of V^{4+} have to be expected (21). This indicates that sample $Mg_1V_4(p)$ is already thermally reduced by heating in an inert atmosphere. Upon switching to reactant-gas mixture at 773 K, the band intensity increases in the region of 300–350 nm, which is probably due to the deposition of weakly condensed polyenyl species being coke precursors (27) (Fig. 9b). Such carbonaceous residues have been detected, too, on the used catalysts by FTIR microscopy. From the different *in situ* studies it can be concluded that the VO^{3+} sites in catalyst $Mg_1V_4(p)$ are markedly reduced to VO^{2+} species, which obviously improve the catalytic performance.

The situation is different for catalyst $Mg_1V_1(c)$. By *in situ* EPR only a small broad singlet of weakly interacting VO^{2+} species is detected at the beginning of the ODH

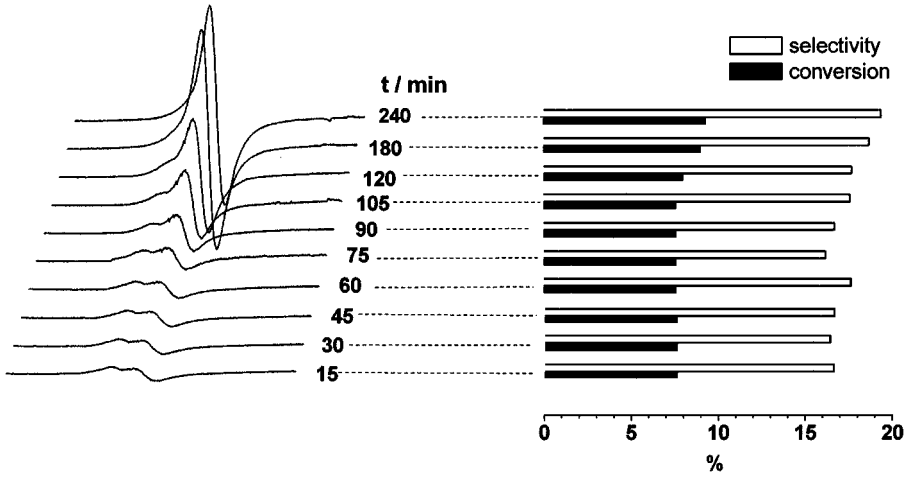

FIG. 8. *In situ* EPR spectra of sample $Mg_1V_4(p)$ during propane ODH at 773 K and corresponding catalytic data obtained by on-line GC.

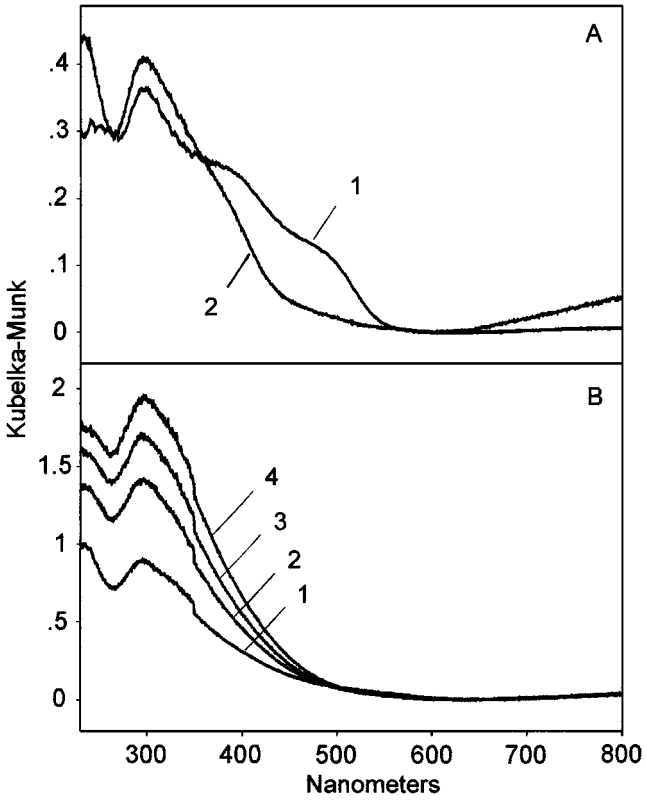

FIG. 9. *In situ* UV/VIS-DRS spectra of Mg_1V_4(p) at room temperature (A) before (1) and after heating in nitrogen flow to 773 K (2) and under propane ODH conditions (B) at 773 K after 5 min (1), 60 min (2), 120 min (3), and 240 min (4) time on stream.

experiment, the intensity of which remains almost constant upon time on stream, indicating that no additional VO^{2+} species are formed. In contrast, *quasi in situ* XPS measurements revealed that after the ODH experiment 43% of the surface V^{5+} sites is reduced to V^{4+} (Table 3). Since these species do obviously not contribute to the EPR spectrum, it is supposed that their coordination is probably tetrahedral. With respect to the overall vanadium content of sample Mg_1V_1(c), the percentage of V^{4+} formed upon reaction is much smaller than that in sample Mg_1V_4(p) since almost no changes are observed in the respective *in situ* UV/VIS spectra. Moreover, the mean vanadium valence in sample Mg_1V_1(p) showing a behavior very similar to that of sample Mg_1V_1(c) changes only from 4.91 before to 4.87 after the catalytic test. All these results suggest that tetrahedrally coordinated V^{5+} species in Mg pyrovanadate are less easily reduced than octahedral VO^{3+} species, being present in V_2O_5 and MgV_2O_6.

4. *Relations between Catalytic Behavior and Structural Properties*

Surface area specific rates of propane conversion and propene formation as well as propene selectivities are plotted for all catalysts in Figs. 10 and 11. Since catalytic activity is a function of the surface vanadium concentration, the values have been normalized with respect to the total vanadium content for deriving explicit relations between the nature of the individual vanadium sites and the catalytic properties by eliminating the influence of different surface vanadium concentrations. This could be done since XPS measurements indicated that the metal/vanadium ratio on the surface is roughly the same as that in the bulk, pointing to a homogeneous distribution throughout the whole sample. Thus, the values on the left ordinate axis in Figs. 10 and 11 are proportional to turnover numbers, which could not be determined directly. Furthermore, it has to be noted that the catalytic tests for Zn–V–O and Pb–V–O samples were performed at 823 K since these solids were found to be not

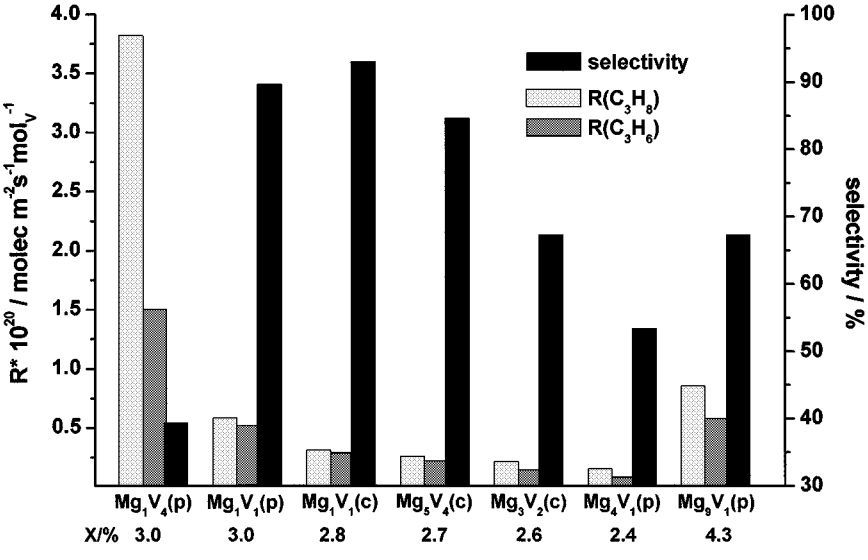

FIG. 10. Area specific rates of propane conversion and propene formation normalized on the total vanadium content and propene selectivities at 773 K for Mg–V–O catalysts (degree of conversion listed in the bottom line).

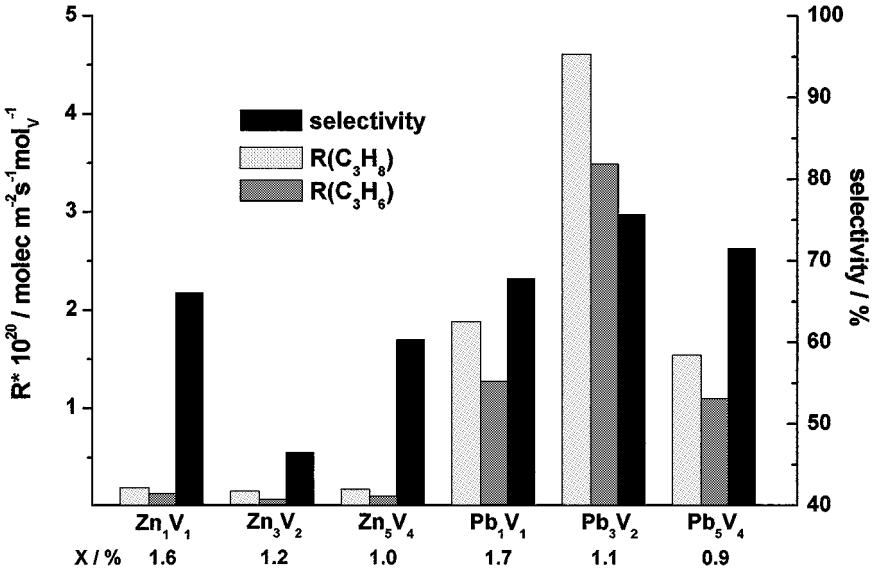

FIG. 11. Area specific rates of propane conversion and propene formation normalized on the total vanadium content and propene selectivities at 823 K for Zn–V–O and Pb–V–O catalysts (degree of conversion listed in the bottom line).

yet active at a temperature of 773 K used to examine the catalytic behavior of Mg–V–O catalysts.

Within the group of Mg–V–O catalysts, sample Mg_1V_4(p), which consists of V_2O_5 and MgV_2O_6, both containing octahedrally coordinated polymerized V^{5+} sites, is most active but poorly selective (Fig. 10). The next active catalyst is Mg_9V_1(p) for which EPR and UV/VIS measurements indicated, besides tetrahedral V^{5+}, the presence of certain amounts of octahedrally coordinated V^{5+} and V^{4+}, which are probably located in an VO_x overlayer on the MgO phase. However, in contrast to sample Mg_1V_4(p) in which only 8.3% of all vanadium sites are tetravalent, the relative percentage of V^{4+} is markedly higher in sample Mg_9V_1(p). Moreover, the VO_x species in the latter catalyst are less polymerized. Both properties, less effective clustering and high relative V^{4+} content, which lowers the oxidation potential, might be regarded as a reason for the higher propene selectivity though lower activity in comparison to sample Mg_1V_4(p). In addition, pyridine adsorption experiments by FTIR have shown that surface acidity is lowest for sample Mg_9V_1(p) and highest for Mg_1V_4(p), which might hinder the propene desorption and lower the selectivity of this catalyst. This is in line with results of Blasco and López-Nieto (1) who observed decreasing olefin selectivities with increasing surface acidity on a variety of supported VO_x catalysts in the ODH of propane and *n*-butane while this effect is not as pronounced for ethane ODH since desorption of the less basic ethylene is also favored from weakly acidic sites. The lower catalytic performance of sample Mg_4V_1(p) in comparison to that of Mg_9V_1(p) could be due to the fact that crystalline MgO, assumed to be associated with an active VO_x overlayer, is only a minor trace component besides Mg orthovanadate in sample Mg_4V_1(p).

Pure Mg ortho- and pyrovanadate, which both contain, besides traces of octahedral VO^{2+} (detected by EPR), only $V^{5+}O_4$ tetrahedra either as isolated units (Mg_3V_2(c)) or connected in pairs (Mg_1V_1(c, p)), are markedly less active but show higher selectivities than the two catalysts discussed above (Fig. 10). Mg_1V_1(c) and Mg_1V_1(p) are somewhat more selective than Mg_3V_2(c). Mg_5V_4(c), which contains a mixture of Mg ortho- and pyrovanadate, takes an intermediate position. The slightly higher activity of sample Mg_1V_1(p) in comparison to that of Mg_1V_1(c) may be due to the smaller crystallite size of the former. However, the different preparation procedures are obviously only of minor influence on the catalytic properties.

Upon comparison of the catalytic results of catalysts Me_1V_1, Me_3V_2, and Me_5V_4 (Me = Mg, Zn, Pb) containing vanadate ions of similar structure, it is evident that the different metal cations have a strong influence. Both activity and selectivity decrease in the order Mg–V–O > Pb–V–O $\gg$ Zn–V–O. This is in contrast to the relationship between dropping ODH selectivities and increasing oxidation potentials of the metal cations established by Kung and Kung (8) for a number of metal orthovanadates in the ODH of butane. With respect to this relationship, a selectivity order of Mg–V–O > Zn–V–O > Pb–V–O should be expected since the oxidation potentials of the cations increase in the order $Mg/Mg^{2+} < Zn/Zn^{2+} < Pb/Pb^{2+}$ (28). This is in contrast to the experimental results. It is also not consistent with the reducibility of the catalysts reflected by the temperature of the TPR onset (Table 2). If this property was of major influence on the propene selectivity, Zn–V–O

samples should be the most selective catalysts. However, it has to be taken into account that in most of the catalysts studied in this work vanadium does form not only *Me*–O–V bonds like in pure orthovanadates but also V–O–V bonds, which could be reduced easier. Thus, the redox properties cannot only be discussed in terms of the oxidation potential of the metal cations. However, the reducibility of the catalysts reflected by the temperature of the TPR onset (Table 2) is also not sufficient to explain the differences in the catalytic performance. Obviously, there are more striking factors than the redox properties that govern the selectivity of metal vanadate catalysts, e.g., the surface acidity. As revealed by TPDA investigations (Table 4), the concentration of acidic sites, in particular of strong ones, is markedly higher on the surface of Zn_1V_1 in comparison to that on Mg_1V_1(c). This could be the reason for the lower selectivity. In contrast, no acidic sites have been detected on Pb_1V_1 by pyridine adsorption. Moreover, the concentration of basic sites is by about a factor of 3 higher on Zn_1V_1 than on Mg_1V_1(c). Such sites are assumed to promote H-abstraction from the propane molecule in the rate-determining step and, thus, improve catalytic activity (9). However, despite more basic surface sites and higher oxidation potential, Zn–V–O catalysts are poorly active in comparison to Mg–V–O catalysts. A reason may be that Zn–V–O samples form much larger crystallites and, thus, show lower defect concentration and structural disorder as detected by XRD and TEM measurements.

Pb–V–O catalysts show comparable selectivities as the corresponding Mg–V–O samples; however, they are less active (Fig. 11). This could be due to the rather high amount of V^{4+} in these samples, which is most probably tetrahedrally coordinated. Thus, it is likely that the oxidation potentials of Pb–V–O catalysts are lower than those of the respective Mg–V–O compounds, which in turn, should give rise to lower activities. In general, *in situ* reduction of V^{5+} to V^{4+} under ODH conditions as detected experimentally, e.g., for samples Mg_1V_4(p) and Mg_1V_1(c), is presumably of important influence on the catalytic performance insofar as it tailors the redox potential of the active surface sites.

CONCLUSIONS

By comparison of the results of catalyst characterization with those of the catalytic tests, it is evident that structure–reactivity relationships in metal vanadate catalysts are rather complex and require consideration of the combined action of different properties such as concentration of acidic and basic surface sites, crystal size, disorder, coordination, and valence state of the vanadium species, which in turn depend on the particular metal ion. Although there is no simple relation between these properties and the catalytic performance, some key features can be derived from the results presented in this work.

Vanadium catalyzes the ODH of propane in both valence states, V^{5+} and V^{4+}; however, V^{4+} seems to be more selective though less active than V^{5+} due to the lower oxidation potential. This can be concluded by comparing the two most active catalysts Mg_1V_4(p) and Mg_9V_1(p) with the lowest and highest fraction of V^{4+} in the total vanadium content. Moreover, *in situ* reduction of V^{5+} to V^{4+} might optimize the surface redox potential under ODH conditions. This issue is frequently not considered in the literature since in most papers only V^{5+} sites are discussed as being active and selective sites (1).

V sites in octahedral or square pyramidal coordination are more active but less selective than VO_4 tetrahedra, probably due to the higher number of coordinating oxygen atoms available for the reaction with the hydrocarbon molecule. This can be concluded by comparing the activity of samples Mg_1V_4(p) and Mg_9V_1(p) with a certain amount of higher coordinated vanadium sites in comparison to that of samples Mg_1V_1(c, p), Mg_3V_2(c), and Mg_5V_4(c) in which almost only tetrahedrally coordinated vanadium has been detected. It is in line with observations of Blasco and López Nieto for a variety of supported VO_x catalysts (1).

Isolated VO_4 and V_2O_7 units as present in crystalline metal ortho- and pyrovanadates, respectively, are more selective but less active than VO_x species connected in clusters (Mg_9V_1(p)) or even in crystalline chain- or layer-like structures (Mg_1V_4(p)).

The differences in the catalytic properties brought about by the different metal ions (Mg^{2+}, Zn^{2+}, Pb^{2+}) are not only governed by the oxidation potential of the latter, as concluded by Kung and Kung (8) for a number of metal orthovanadates in the ODH of *n*-butane, but to a major degree also by the acid–base properities and the crystal size and the extent of structural disorder. Thus, it seems likely that the low activity of Zn–V–O catalysts is mainly a consequence of the large crystal size and low defect concentration, notwithstanding the fact that the oxidation potential of Zn/Zn^{2+} is higher than that of Mg/Mg^{2+} and the concentration of basic surface sites promoting the rate-determining H-abstraction is higher in Zn–V–O, too. The selectivities of Pb–V–O catalysts are only slightly lower compared to those of Mg–V–O compounds, although the oxidation potential of Pb/Pb^{2+} is about 20 times larger than that of Mg/Mg^{2+}. A possible reason therefore could be the rather high percentage of tetravalent vanadium in the Pb–V–O samples, which retains high selectivities, however, at the expense of activity.

As a main conclusion of the investigations in this work, it appears promising to use supported vanadia catalysts with highly dispersed, preferably tetrahedrally coordinated, V^{5+} sites to achieve high selectivities. The inherently lower activities should be compensated for by using high surface area supports of low surface acidity. First promising results were obtained with a supported VO_x/MCM catalyst (29),

which is known to possess the properties mentioned above (30).

ACKNOWLEDGEMENTS

The authors thank Dr. U. Bentrup for performing the pyridine adsorption measurements and the DFG for financial support (Grant Br 1380/4-1).

REFERENCES

1. Blasco, T., and López-Nieto, J. M., *Appl. Catal.* **157**, 117 (1997).
2. Banares, M. A., *Catal. Today* **51**, 319 (1999).
3. Mamedov, E. A., and Cortés Coberán, V., *Appl. Catal. A* **127**, 1 (1995).
4. Chaar, M., Patel, D., and Kung, H. H., *J. Catal.* **109**, 463 (1988).
5. Michalakos, P. M., Kung, M. C., Jahan, I., and Kung, H. H., *J. Catal.* **140**, 226 (1993).
6. Siew Hew Sam, D., Soenen, V., and Volta, J. C., *J. Catal* **123**, 417 (1990).
7. Guerrero-Ruiz, A., Rodriguez-Ramos, I., Fierro, J. L. G., Soenen, V., Herrmann, J. M., and Volta, J. C., *in* "Novel Development in Selective Oxidation by Heterogeneous Catalysis" (P. Ruiz and B. Delmon, Eds.), Vol. 72, p. 203. Elsevier, Amsterdam, 1992.
8. Kung, H. H., and Kung, M. C., *Appl. Catal. A* **157,** 105 (1997).
9. Pantazidis, A., Aurox, A., Herrmann, J. M., and Mirodatos, C., *Catal. Today* **32**, 81 (1996).
10. Gao, X., Ruiz, P., Xin, Q., Guo, X., and Delmon, B., *J. Catal.* **148**, 56 (1994).
11. Burrows, A., Kiely, C. J., Perregaard, J., Højlund-Nielsen, P. E., Vorbeck, G., Calvino, J. J., and López-Cartes, C., *Catal. Lett.* **57**, 121 (1999).
12. Niwa, M., and Murakami, Y., *J. Catal.* **76**, 9 (1982).
13. Brückner, A., Kubias, B., Lücke B., and R. Stößer, *Colloids Surf.* **115**, 179 (1996).
14. Karge, H. G., Lange, J. P., Gutze A., and Laniecki, M., *J. Catal.* **114**, 144 (1988).
15. Dyrek, K., Madej, A., Mazur, E., and Rokosz, A., *Colloids Surf.* **45**, 135 (1990).
16. Scofield, J. H., *J. Electron Spectrosc.* **8**, 129 (1976).
17. Koranne, M. M., Goodwin, J. G., and Marcelin, G., *J. Catal.* **148**, 369 (1994).
18. Moulder, J. F., Stickle, W. F., Sobol, P. E., and Bomben, K. D., *in* "Handbook of X-ray Photoelectron Spectroscopy" (J. Chastain and R. C. King Jr., Eds.). p. 241. Physical Electronics Inc., Eden Prairie, 1995.
19. Unger, W., Gross, Th., Böse, O., Fritz, Th., and Gelius, U., *Nachrichten Chem.* **48**, 1108 (2000).
20. Vedrine, J. C., *in* "Characterization of Heterogeneous Catalysts" (F. Delannay, Ed.), p. 161. Dekker, New York, 1984.
21. Centi, G., Perathoner, S. and Trifiró, F., *J. Phys. Chem.* **96**, 2617 (1992).
22. Schraml-Marth, M., Wokaun, A., Pohl, M., and Krauss, H.-L., *J. Chem. Soc. Faraday Trans.* **87**, 2635 (1991).
23. Morey, M., Davidson, A., Eckert, H., and Stucky, G., *Chem. Mater.* **8**, 486 (1996).
24. Brückner, A., *Appl. Catal. A* **200**, 287 (2000).
25. Oganowski, W., Hanuza, J., and Jezowska-Trzebiatowska, B., *Bull. Pol. Acad. Sci.* **32**, 355 (1984).
26. Pantazidis, A., Burrows, A., Kiely, C. J., and Mirodatos, C., *J. Catal.* **177**, 325 (1998).
27. Karge, H. G., Laniecki, M., Ziolek, M., Onyestyak, G., Kiss, A., Kleinschmit, P., and Siray, M., *Zeolites: Facts Figures Future* 1327 (1989).
28. "Handbook of Chemistry and Physics," 75th ed. CRC Press, Boca Raton, FL, 1994.
29. Buyevskaya, O. V., Brückner, A., Kondratenko, E. V., Wolf, D., and Baerns, M., *Catal. Today*, in press.
30. Berndt, H., Martin, A., Brückner, A., Schreier, E., Müller, D., Kosslick, H., Wolf, G.-U., and Lücke, B., *J. Catal.* **191**, 384 (2000).